Improving exchange-spring nanocomposite permanent magnets

J. S. Jiang, J. E. Pearson, Z. Y. Liu, B. Kabius, S. Trasobares, D. J. Miller, and S. D. Bader
Materials Science Division, Argonne National Laboratory, Argonne, Illinois 60439

D. R. Lee, D. Haskel, and G. Srajer
Advanced Photon Source, Argonne National Laboratory, Argonne, Illinois 60439

J. P. Liu
Department of Physics, University of Texas at Arlington, Arlington, Texas 76019

(Received 8 July 2004; accepted 28 September 2004)

We demonstrate a counterintuitive approach for improving exchange-spring magnets. Contrary to the general belief that the exchange–spring interface must be ideal and atomically coherent, we thermally process, by annealing or high-temperature deposition, epitaxial Sm–Co/Fe thin-film bilayers to induce interfacial mixing. Synchrotron x-ray scattering and electron microscopy elemental mapping confirm the formation of a graded interface. The thermal processing enhances the nucleation field and the energy product. The hysteresis loop becomes more single-phase-like yet the magnetization remains fully reversible. Model simulations produce demagnetization behaviors similar to experimental observations. © *2004 American Institute of Physics*.
[DOI: 10.1063/1.1828225]

The "exchange-spring" mechanism in nanocomposite magnets,[1] where the interfacial exchange coupling between the magnetically soft and hard phases hardens the soft phase and enhances remanence and reversibility, could lead to ultrastrong permanent magnets whose energy product $(BH)_{\max}$ is more than twice that of Nd–Fe–B.[2] However, exchange-spring magnets have yet to deliver on the promise of significantly enhanced properties. The basic tenets for maximizing exchange spring performance have been that the soft grains be comparable to the hard-phase domain-wall width,[1] and that the grain boundaries be ideal,[3] both of which aim to achieve effective interphase coupling. Limiting soft grain growth in magnet processing is generally accomplished with nonmagnetic additives, at the expense of forming grain boundary phases that reduce interfacial coupling and the overall magnetization.[4,5] Although increasing the interfacial coupling strength can improve coupling effectiveness,[6,7] such improvement is fundamentally limited by the physics of magnetization reversal. This is because even for an ideal exchange–spring interface, the soft moments remain parallel to the hard ones only at fields below the exchange field H_{ex}, which is the upper limit for the nucleation field H_N—a more general technical term denoting the onset of magnetic reversal and the limiting factor for $(BH)_{\max}$. H_{ex} is given by the soft phase exchange constant and thickness;[8] for an exchange spring with 200 Å of Fe as the soft phase, $H_{ex} \cong 2$ kOe. Improving epitaxy or interfacial coupling does not overcome this limit.

In this letter, we report an effective pathway via interfacial properties modification to increase H_N, and hence $(BH)_{\max}$, of exchange-spring magnets. We demonstrate such tailoring via thermally processed epitaxial Sm–Co/Fe and Sm–Co/Co bilayer structures. In contrast to Refs. 7 and 9, we start with an exchange spring where the interface is already ideal, and create a graded interfacial region where the material parameters vary gradually by promoting intermixing of Sm–Co with Fe or Co. Such an interfacial modification fundamentally changes the magnetization behavior. We discuss its applicability and implication on magnet processing toward realizing the full potential of the exchange spring principle.

We fabricated the Sm–Co/Fe and Sm–Co/Co exchange-spring bilayess by dc magnetron sputtering. These bilayers are a model exchange-spring system with ideal, coherent interfaces.[10,11] The nominally Sm_2Co_7 layer was grown epitaxially at 400 °C onto a Cr(211)-buffered single crystal MgO(110) substrate to achieve an in-plane uniaxial anisotropy, as described in Ref. 10. The thickness of the Sm–Co layer in all samples was kept at 200 Å. Following the deposition of the Sm–Co hard layer, Fe or Co soft layers were either deposited at 70–100 °C, or immediately at 400 °C. The Fe or Co layers are 100 and 200 Å in thickness. All samples were capped with 10 nm of Ag or Ag(5 nm)/Cr(5 nm) cover layers. Pieces were cut from the as-deposited samples and were annealed for 1 h at temperatures ranging from 200 to 400 °C, using the same heater inside the deposition chamber in a vacuum of 1×10^{-8} Torr. We denote a sample by its substrate temperature T_S or annealing temperature T_A, which is the highest temperature the soft layer was subjected to during processing. No intermixing should occur at the Fe/Ag interface since Fe and Ag are mutually insoluble. And the intrinsic properties of the Sm–Co layer should remain intact because the processing temperatures never exceed the deposition temperature of Sm–Co.

The magnetic properties were measured using an alternating gradient magnetometer with the field applied along the easy direction of the Sm–Co layer. Shown in Fig. 1(a) are the normalized, room-temperature demagnetization curves of three Sm–Co(20 nm)/Fe(20 nm) samples with T_S=70 °C, T_A=300 °C, and T_s=400 °C, respectively. The first sample shows the two-stepped hysteresis loop typical of an exchange-spring with ineffective coupling: the Fe layer starts to reverse at an H_N of ~1 kOe and the Sm–Co layer switches at the irreversibility field $H_{\text{irr}} \sim 7.5$ kOe. These values are identical to those in Ref. 10. The second sample shows that after annealing at 300° C, H_N increases to ~1.2 kOe while H_{irr} is reduced to ~7.2 kOe. For the third

 © 2004 American Institute of Physics

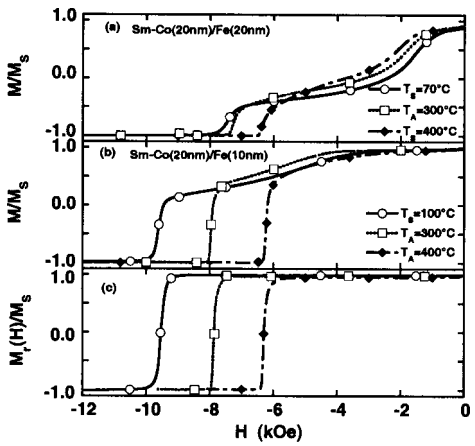

FIG. 1. (a) Normalized room-temperature demagnetization curves for three Sm–Co(20 nm)/Fe(20 nm) samples as-deposited or annealed at various temperatures, (b) demagnetization, and (c) dc demagnetization remanence curves for Sm–Co(20 nm)/Fe(10 nm).

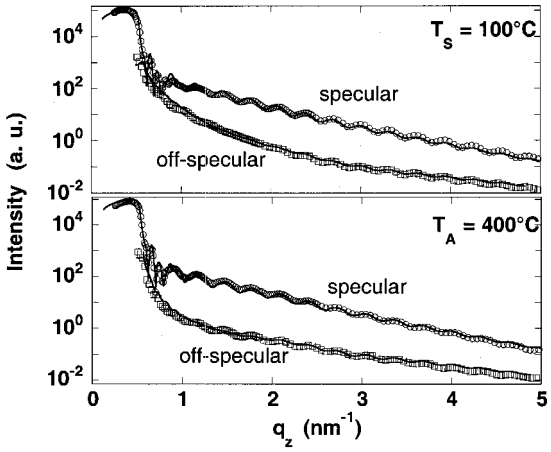

FIG. 2. Specular and off-specular x-ray reflectivity curves of the T_S =100 °C and T_A=400 °C Sm–Co(20 nm)/Fe(10 nm). The off-specular reflectivity was measured with a −0.04° offset. The solid lines are fits.

sample, H_N further increases to 1.6 kOe and H_{irr} decreases to ~6 kOe. We found no discernable difference in its magnetization behavior, eliminating the possibility of contamination (thus reduced coupling) when the Sm–Co was exposed. The saturation magnetization (M_s) for all samples is 1125 emu/cm^3. The increase in H_N increases $(BH)_{max}$ from 9.4 MGOe for the T_S=70 °C sample, to 12 MGOe at T_A =300 °C, to 14.1 MGOe at T_S=400 °C.

Thermal processing caused more pronounced changes in samples with thinner Fe layers. Shown in Fig. 1(b) are the demagnetization curves for Sm–Co(20 nm)/Fe(10 nm) samples with T_S=100 °C, T_A=300 °C, and 400 °C, respectively. At T_A=300 °C, H_N increases to over 4 kOe, while H_{irr} decreases. After annealing at 400 °C, the magnetization becomes single-phase-like, with coercivity H_c>6 kOe. The $(BH)_{max}$ value increases from 24 MGOe for the as-deposited sample to 27.7 MGOe at T_A=300 °C, then decreases to 22.4 MGOe at T_A=400 °C. Note that although the mathematical limit of $(BH)_{max}$ for Sm–Co/Fe of this composition is 34 MGOe, $(BH)_{max}$ is only 21 MGOe for an ideal exchange spring because Fe reversal at H_{ex} decreases the magnetization.[10] Annealing has made up nearly 50% of the difference. The dc demagnetization remanence (DCD) curves, which measure the reversibility of the magnetization, are shown in Fig. 1(c). For the DCD curves, the samples were saturated with a +1.4 T field each time before a demagnetizing field was applied. All samples have sharp step-like DCD curves, indicating a narrow distribution in the hard-layer switching field and full reversibility of the soft layer magnetization. Particularly noteworthy is that the T_A =400 °C sample has a nearly square demagnetization curve, yet the magnetization is fully reversible. In contrast, most nanophase hard magnets show significant irreversible demagnetization behavior due to partial reversal of the hard phase, even if their hysteresis loops may appear single-phase-like.[4,9]

The effect of annealing on the interfacial morphology and crystal structure has been characterized by x-ray scattering and by energy-filtered transmission electron microscopy (EFTEM). Figure 2 shows the specular and off-specular reflectivity measured using 7-keV-synchrotron radiation (λ =0.17712 nm) on two Sm–Co(20 nm)/Fe(10 nm) samples, with T_S=100 °C and with T_A=400 °C. The specular reflectivity curves for both samples are very similar while the T_S =100 °C sample shows higher off-specular intersity at low q_z. Fits to the specular reflectivity curves give similar total interface width (roughness and interdiffusion) of ~2.5 nm for both samples. On the other hand, fits to the off-specular intensity using a distorted-wave Born approximation (DWBA) model[12] give different roughness amplitudes of 2.0 and 0.7 nm, respectively. When the Fe layer is deposited at a low temperature, the Sm–Co/Fe interface is sharp but jagged. Annealing or depositing the Fe layer at elevated temperatures promotes interdiffusion between the Sm–Co and Fe, blurring the interface and reducing the roughness.

This evolution in microstructure is immediately evident in the cross-sectional EFTEM images shown in Fig. 3 for two Sm–Co(20 nm)/Fe(20 nm) samples with T_S=100 °C, and T_A=400 °C. The images are constructed from the electron energy loss spectra (EELS) at characteristic absorption energies of Fe, Co, and Cr, and color coded to represent the spatial distribution of the elements. The resolution is 0.5 nm. The Co map (red) shows the notch in the T_S=100 °C sample due to interfacial roughness, whereas the T_A=400 °C sample

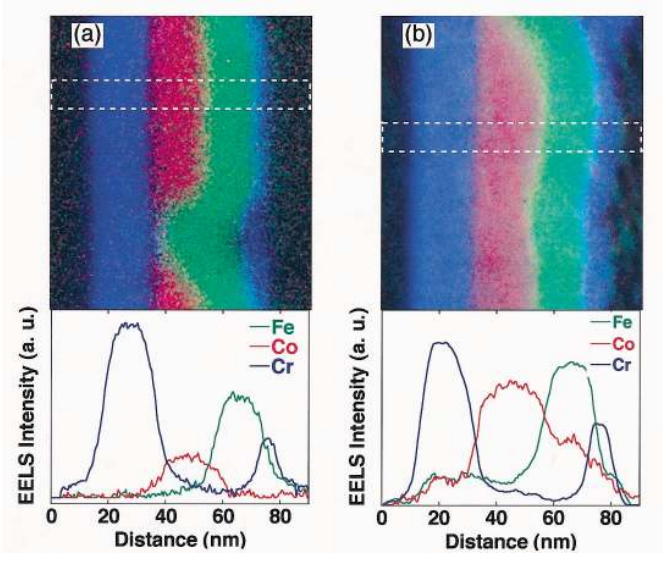

FIG. 3. (Color) EELS elemental maps and line scans of Sm–Co(20 nm)/Fe(20 nm) samples with (a) T_S=100 °C and (b) T_A =400 °C. The line scans are taken from the area enclosed by the dashes.

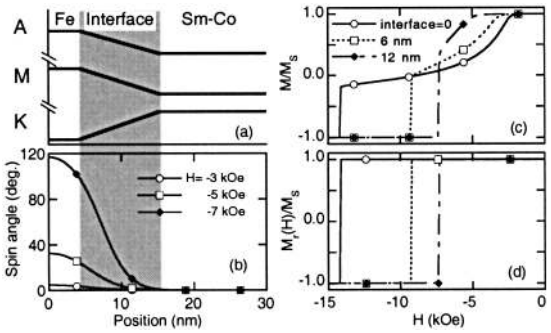

FIG. 4. (a) Schematic illustration of the exchange (A), anisotropy (K) and magnetization (M) across a graded Sm–Co/Fe interface; (b) calculated spin profile of a Sm–Co(20 nm)/Fe(10 nm) bilayer with a 12-nm-interfacial region at various reversal fields; (c) the demagnetization and (d) the dc demagnetization remanence curves calculated for Sm–Co(20 nm)/Fe(10 nm) bilayers with interfacial regions of various thickness.

has a diffuse boundary between the Fe (green) and Co maps and a notch is blurred out. The difference in interdiffusion in the samples can be seen more clearly in the 9-nm-wide line scans. In the T_S=100 °C sample the layers are well defined, but in the T_A=400 °C sample Fe is found in the entire Sm–Co layer while the amount of Co entering into the Fe layer decreases with distance from the interface. High angle x-ray diffraction of the T_A=400 °C sample shows a broad shoulder to the right of the Sm–Co($2\bar{2}00$) peak. The shoulder could not be fitted with a single Gaussian curve, suggesting a distribution of phases with smaller lattice constants.

To correlate the microstructural evolution with the observed changes in magnetic properties, we simulated the demagnetization behavior of these bilayers using the one-dimensional spin-chain model described in Ref. 10. Based on the x-ray diffraction results, intermixing of Sm–Co and Fe likely creates pseudobinary intermetallic Sm–(Co,Fe) compounds. Past studies of the $Sm_2(Co_{1-x}Fe_x)_{17}$ alloy phase have found that incorporation of Fe increases the magnetization, and that the Curie temperature varies continuously with x.[13,14] We therefore model the interdiffused interface with a graded profile for the intrinsic material parameters, where the exchange constant A, the magnetic anisotropy K, and the magnetization M ramp linearly, from those of the Fe to those of the Sm–Co, as depicted in Fig. 4(a). The end values for A, K, and M are the same as those used for Fe and Sm–Co in Ref. 10, and the width of the interfacial region reflects the extent of interdiffusion. The results for three Sm–Co(20 nm)/Fe(10 nm) bilayers with different interface widths are plotted in Figs. 4(c) and 4(d). The simulated demagnetization and DCD curves closely resemble those measured experimentally. The measured demagnetization curve becomes more single-phase-like with increased annealing temperature, and the same trend is seen in the simulated loops for increased interface width. The results of intermixing are that the anisotropy increases and magnetization decreases in the part of the interfacial region which used to be soft Fe, leading to an increase of H_N, and that the improved coupling effectiveness and the reduced anisotropy in the modified hard region combine to lower H_{irr}.

The numerical simulations also reveal additional important advantages of a graded interface that suggest improved magnetic stability. Figure 4(b) shows the simulated spin profile of a modified Sm–Co(20 nm)/Fe(10 nm) bilayer with a 12-nm-thick interfacial region at various reverse fields. The magnetic reversal is always confined in the interfacial region, leaving the hard layer undisturbed. In contrast, in exchange-spring bilayers with abrupt interfaces, the reversal extends into the hard layer,[10] leading to magnetic instability against field cycling when the hard layer is thin.[15]

We note that for the Sm–Co/Co bilayers, annealing yields no systematic variation in the loop shape, but generally reduces the nucleation field. Sm–Co exists in many discrete metastable phases;[16] annealing Sm–Co/Co might locally change the composition[17] and create stepwise material parameter profiles similar to those in Ref. 9. It is therefore essential to create a graded interface where the material parameters do not vary abruptly in order to improve the effectiveness of the exchange spring coupling. Such a profile might be accomplished by selecting material components that form solutions upon annealing, or by athermal means that can modify the interface in a nonequilibrium fashion.

In conclusion, we demonstrate a strategy to overcome the difficulties of traditional magnet processing in realizing the full potential of exchange-spring magnets. Annealing or depositing Sm–Co/Fe bilayers at high temperatures induces intermixing at the interface and increases the nucleation field, hence improving the energy product. We modeled the effect of thermal processing with a graded interfacial region and qualitatively reproduced the experimental observations. The graded interface keeps the hard phase undisturbed during reversal, leading to potentially improved magnetic stability.

Work at Argonne was supported by the U.S. DOE BES-MS Contract No. W-31-109-ENG-38. The authors thank Y. Choi for assistance with the reflectivity measurements. EFTEM was carried out at Argonne's Electron Microscopy Center. J.P.L. was supported by the U.S. DOD/DARPA Grant No. DAAD 19-01-1-0546.

[1]E. F. Kneller and R. Hawig, IEEE Trans. Magn. **27**, 3588 (1991).
[2]R. Skomski and J. M. D. Coey, Phys. Rev. B **48**, 15812 (1993).
[3]R. Fischer and H. Kronmüller, J. Appl. Phys. **83**, 3271 (1998).
[4]G. C. Hadjipanayis, J. Magn. Magn. Mater. **200**, 373 (1999).
[5]A. Zern, M. Seeger, J. Bauer, and H. Kronmüller, J. Magn. Magn. Mater. **184**, 89 (1998).
[6]T. Nagahama, K. Mibu, and T. Shinjo, J. Phys. D **31**, 43 (1998).
[7]J. Kim, K. Barmark, M. De Graef, L. H. Lewis, and D. C. Crew, J. Appl. Phys. **87**, 6140 (2000).
[8]E. Goto, N. Hayashi, T. Miyashita, and K. Nakagawa, J. Appl. Phys. **36**, 2951 (1965).
[9]D. C. Crew, J. Kim, L. H. Lewis, and K. Barmak, J. Magn. Magn. Mater. **233**, 257 (2001).
[10]E. E. Fullerton, J. S. Jiang, and S. D. Bader, J. Magn. Magn. Mater. **200**, 392 (1999).
[11]M. J. Pechan, N. Teng, J.-D. Stewart, J. Zachary Hilt, E. E. Fullerton, J. S. Jiang, C. H. Sowers, and S. D. Bader, J. Appl. Phys. **87**, 6686 (2000).
[12]D. R. Lee, Y. J. Park, D. Kim, Y. H. Jeong, and K.-B. Lee, Phys. Rev. B **57**, 8786 (1998).
[13]A. E. Ray and K. J. Strnat, IEEE Trans. Magn. **MAG-8**, 516 (1972).
[14]K. J. Strnat, and R. M. W. Strnat, J. Magn. Magn. Mater. **100**, 38 (1991).
[15]A. Inomata, J. S. Jiang, C. Y. You, J. E. Pearson, and S. D. Bader, J. Vac. Sci. Technol. A **18**, 1269 (2000).
[16]K. H. J. Buschow, in *Supermagnets, Hard Magnetic Materials*, edited by G. J. Long and F. Grandjean (Kluwer, Dordrecht, 1991), p. 553.
[17]J. P. Liu, Y. Liu, R. Skomski, and D. J. Sellmyer, J. Appl. Phys. **85**, 4812 (1999).